BAMS Article

Extreme Precipitation on Consecutive Days Occurs More Often in a Warming Climate

Haibo Du, Markus G. Donat, Shengwei Zong, Lisa V. Alexander, Rodrigo Manzanas, Andries Kruger, Gwangyong Choi, Jim Salinger, Hong S. He, Mai-He Li, Fumiaki Fujibe, Banzragch Nandintsetseg, Shafiqur Rehman, Farhat Abbas, Matilde Rusticucci, Arvind Srivastava, Panmao Zhai, Tanya Lippmann, Ibouraïma Yabi, Michael C. Stambaugh, Shengzhong Wang, Altangerel Batbold, Priscilla Teles de Oliveira, Muhammad Adrees, Wei Hou, Claudio Moises Santos e Silva, Paulo Sergio Lucio, and Zhengfang Wu

ABSTRACT: Extreme precipitation occurring on consecutive days may substantially increase the risk of related impacts, but changes in such events have not been studied at a global scale. Here we use a unique global dataset based on in situ observations and multimodel historical and future simulations to analyze the changes in the frequency of extreme precipitation on consecutive days (EPCD). We further disentangle the relative contributions of variations in precipitation intensity and temporal correlation of extreme precipitation to understand the processes that drive the changes in EPCD. Observations and climate model simulations show that the frequency of EPCD is increasing in most land regions, in particular, in North America, Europe, and the Northern Hemisphere high latitudes. These increases are primarily a consequence of increasing precipitation intensity, but changes in the temporal correlation of extreme precipitation regionally amplify or reduce the effects of intensity changes. Changes are larger in simulations with a stronger warming signal, suggesting that further increases in EPCD are expected for the future under continued climate warming.

KEYWORDS: Extreme events; Precipitation; Climate change; Climate records; Climate prediction

https://doi.org/10.1175/BAMS-D-21-0140.1
Corresponding author: Dr. Haibo Du, duhb655@nenu.edu.cn; Dr. Markus Donat, markus.donat@bsc.es
Haibo Du and Markus G. Donat contributed equally to this work.
Supplemental material: https://doi.org/10.1175/BAMS-D-21-0140.2
In final form 1 December 2021

AFFILIATIONS: Du—Key Laboratory of Geographical Processes and Ecological Security in Changbai Mountains, Ministry of Education, School of Geographical Sciences, and Key Laboratory of Vegetation Ecology, Ministry of Education, Northeast Normal University, Changchun, China; **Donat**—Barcelona Supercomputing Center, and ICREA, Barcelona, Spain; **Zong and Wang**—Key Laboratory of Geographical Processes and Ecological Security in Changbai Mountains, Ministry of Education, School of Geographical Sciences, Northeast Normal University, Changchun, China; **Alexander**—Climate Change Research Centre, and ARC Centre of Excellence for Climate Extremes, University of New South Wales, Sydney, New South Wales, Australia; **Manzanas**—Meteorology Group, Departamento de Matemática Aplicada y Ciencias de la Computación, Universidad de Cantabria, Santander, Spain; **Kruger**—Climate Service Department, South African Weather Service, and Department of Geography, Geoinformatics and Meteorology, Faculty of Natural and Agricultural Sciences, University of Pretoria, Pretoria, South Africa; **Choi**—Geography Education, Jeju National University, Jeju-si, Jeju, South Korea; **Salinger**—School of Geography, Environment and Earth Sciences, Victoria University of Wellington, Wellington, New Zealand; **He**—School of Natural Resource, University of Missouri, Columbia, Missouri, and Key Laboratory of Geographical Processes and Ecological Security in Changbai Mountains, Ministry of Education, School of Geographical Sciences, Northeast Normal University, Changchun, China; **Li**—Key Laboratory of Geographical Processes and Ecological Security in Changbai Mountains, Ministry of Education, School of Geographical Sciences, Northeast Normal University, Changchun, China, and Swiss Federal Research Institute (WSL), Birmensdorf, Switzerland; **Fujibe**—Department of Geography, Tokyo Metropolitan University, Hachioji, Japan; **Nandintsetseg**—Eurasia Institute of Earth Sciences, Istanbul Technical University, Istanbul, Turkey, and Information and Research Institute of Meteorology, Hydrology and Environment, Ulaanbaatar, Mongolia, and Graduate School of Environmental Studies, Nagoya University, Nagoya, Japan; **Rehman**—Interdisciplinary Research Center for Renewable Energy and Power Systems, Research Institute, King Fahd University of Petroleum and Minerals, Dhahran, Saudi Arabia; **Abbas**—School of Climate Change and Adaptation, University of Prince Edward Island, Charlottetown, Prince Edward Island, Canada; **Rusticucci**—Departamento de Ciencias de la Atmósfera y los Océanos, Universidad de Buenos Aires/CONICET, Buenos Aires, Argentina; **Srivastava**—National Climate Centre, India Meteorological Department, Pune, India; **Zhai**—State Key Laboratory of Severe Weather, Chinese Academy of Meteorological Sciences, CMA, Beijing, China; **Lippmann**—Climate Change Research Centre, and ARC Centre of Excellence for Climate Extremes, University of New South Wales, Sydney, New South Wales, Australia, and Department of Earth Sciences, Vrije Universiteit Amsterdam, Amsterdam, Netherlands; **Yabi**—Laboratory "Pierre PAGNEY," Climat, Eau, Ecosystème Développement (LACEEDE), Department of Geography and Planning, University of Abomey-Calavi, Abomey-Calavi, Benin; **Stambaugh**—School of Natural Resource, University of Missouri, Columbia, Missouri; **Batbold**—Information and Research Institute of Meteorology, Hydrology and Environment, Ulaanbaatar, Mongolia; **Oliveira**—School of Sciences, São Paulo State University (UNESP), Bauru, São Paulo, Brazil; **Adrees**—School of Climate Change and Adaptation, University of Prince Edward Island, Charlottetown, Prince Edward Island, Canada, and Department of Environmental Sciences and Engineering, Government College University Faisalabad, Faisalabad, Pakistan; **Hou**—National Climate Center, China Meteorological Administration, Beijing, China; **Silva and Lucio**—Departament of Atmospheric and Climatic Sciences, Graduate Program in Climatic Sciences, Federal University of Rio Grande do Norte, Natal, Brazil; **Wu**—Key Laboratory of Geographical Processes and Ecological Security in Changbai Mountains, Ministry of Education, School of Geographical Sciences, and Key Laboratory of Vegetation Ecology, Ministry of Education, Northeast Normal University, Changchun, China

Precipitation accumulates over variable durations and temporal sequences, which contributes to complexity when studying extremes and their related impacts. Short-lived [e.g., hourly (Barbero et al. 2017) and daily (Westra et al. 2013)] precipitation extremes may cause sudden and small-scale flash flooding, whereas precipitation extremes over several consecutive days may lead to extensive and larger-scale flooding (Kundzewicz et al. 2005; Ulbrich et al. 2003). While Dwyer and O'Gorman (2017) identified a tendency toward slight reduction in the duration of (subdaily) extreme precipitation events, hazardous floods are often associated with continuous periods of persistent heavy rainfall. For example, consecutive multiple-day extreme precipitation events caused severe flooding in central Europe in August 2002 (Ulbrich et al. 2003), as well as in Asia such as China in 1998 (Zong and Chen 2000), Pakistan in 2010 (Webster et al. 2011), Japan in 2018 (Tsuguti et al. 2019), and most recently in central Europe in July 2021 (Kreienkamp et al. 2021). While changes in extreme precipitation accumulation over specific time windows have been extensively studied indicating widespread intensification (Allen and Ingram 2002; Asadieh and Krakauer 2015; Donat et al. 2016, 2013; Du et al. 2013; Fischer and Knutti 2015; Guerreiro et al. 2018; Pfahl et al. 2017), changes in the temporal distribution of precipitation are an important aspect affecting how much water reaches the surface in a given time period (Guilbert et al. 2015; Pfleiderer et al. 2019; Trenberth 2011). The same precipitation totals can result in different impacts on ecosystems or society depending on whether precipitation is concentrated in a few short periods or more equally distributed over longer periods (Zolina et al. 2013). For example, the presence of high-amplitude quasi-stationary atmospheric waves has been linked to different types of climate extremes including persistent episodes of extreme precipitation in the Northern Hemisphere summer (Kornhuber et al. 2019; Wolf et al. 2018).

The observed and simulated widespread intensification of precipitation extremes has been shown to be at first order a consequence of thermodynamic effects, i.e., the anticipated warming and moistening of the atmosphere (Allen and Ingram 2002), and in some regions in combination with lapse-rate changes (O'Gorman and Schneider 2009). However, dynamical effects can regionally modify the changes in extreme precipitation caused by thermodynamic contributions alone, amplifying or weakening the changes (Pfahl et al. 2017). Some studies have further suggested summer weather patterns may become more persistent in a warmer climate (Mann et al. 2017; Pfleiderer et al. 2019), although changes in atmospheric dynamics are among the less robust features of climate model simulations (Shepherd 2014). Such increasing occurrence of specific large-scale weather situations (e.g., quasi-stationary atmospheric waves) in a warmer climate (Mann et al. 2017; Pfleiderer et al. 2019) may create favorable conditions for persistent extremes to occur (Screen and Simmonds 2014). However, to date it is unknown if and how extreme precipitation on consecutive days (EPCD; defined here as a multiday event when daily precipitation exceeds the 99th-percentile threshold on at least two consecutive days) are changing.

Here, we investigate the temporal and spatial changes in EPCD frequency using a unique observational dataset covering most of the global land areas during 1961–2010 except large parts of the tropics (Fig. ES1), as well as global climate model simulations from the Coupled Model Intercomparison Project phase 5 (CMIP5) (Table ES1) and regional climate model simulations from the Coordinated Regional Climate Downscaling Experiment (CORDEX) (Table ES2). Coauthors from fifteen countries have contributed with local to regional data to this novel observational dataset. We further disentangle the effects of precipitation intensification and temporal correlation of extreme precipitation events on the changes in EPCD.

Materials and methods

Observational data. This study uses uniquely combined observed daily precipitation data from a number of different sources, including publicly available datasets [e.g., the Global

Historical Climatology Network-Daily (GHCND) dataset (Menne et al. 2012), the ECA&D dataset (Klein Tank et al. 2002), the USHCN dataset (Menne et al. 2016), and Canada (Vincent et al. 2012)] and data contributed by coauthors from Argentina, Australia, Benin, Brazil, China, India, Japan, Korea, Mongolia, New Zealand, Pakistan, South Africa, Saudi Arabia, Spain, and Russia. Quality control (Alexander et al. 2006) and homogeneity test (Wang and Feng 2013) for each station are completed before further processing. Stations are excluded from the analysis if their data are identified as inhomogeneous. Any year with more than 10% of missing values is treated as a "missing year." Missing values that occur in "dry" months without precipitation extremes are excluded from counting the number of missing values for a year, because missing values in "dry" months do not affect the frequency of EPCD. This also benefits to retain more station data that meet the completeness criteria below. Therefore, we only count the number of missing values in "wet" months. We first calculate the 99th percentile of the whole available daily precipitation during the 50 years 1961–2010. A month is then defined as "wet" if the 99th percentile is exceeded at least once in the 50 years of data in that month. Next, stations with available data for at least 75% of the years during 1961–2010 are retained. This leaves 6,006 high-quality stations with long-term (including 5,000 stations with at least 45 years of data) daily precipitation during 1961–2010 for this study (Fig. ES1). The authors contribute 34% to the observation dataset. We also check the annual percentage of stations with missing data (Fig. ES2). Years with missing data are more often distributed at the beginning and the end of the period. Although the percentage of stations with missing data are not high, it might affect the observed trends in EPCD frequency. Therefore, we test the robustness of the results when excluding stations that have more than 3 years (or 2 years) missing data among the first or last 5 years of the period to reduce the missing value rate (Fig. ES2) to test the potential effects of these missing data on the changes in EPCD frequency (Fig. ES3). This provides us with two alternative, more complete, datasets, consisting of 5,269 (or 5,032) stations after excluding stations with missing data at the beginning and end of the period. The percentage of stations with missing data for these two alternative datasets is very low for all years, except for 2010, in which the percentage is ~11%. We analyze the changes in EPCD frequency for these different datasets and for different periods (1961–2010 and 1961–2009) to test the sensitivity of results to different datasets and periods. The results show that the changes in EPCD frequency are very similar between the three dataset versions and between the two periods (Fig. ES3). Therefore, this study uses the larger set of 6,006 stations to analyze the changes in EPCD frequency for observations. At last, grid cells with available data for at least 90% of the years (i.e., 45 years) are retained to calculate the local and regional changes. Because the observational data are missing in large parts of the tropics, this study analyses observed changes only in the extratropics.

Historical and future climate simulation data. This study uses data from 30 global climate models (GCM) which contributed to the CMIP5, including historical simulations (1961–2005) and future projections (2006–100). Two future representative concentration pathways (RCP8.5 for high-emission scenario and RCP4.5 for medium-emission scenario) are used to simulate changes in extreme precipitation by the end of the twenty-first century (Table ES1). When analyzing the climate model simulations available within CMIP5, we merge the historical and RCP8.5 simulations to have long transient data for 1961–2100. We then analyze the CMIP5 past changes over exactly the same period as observations, i.e., 1961–2010. The 99th-percentile threshold shows a similar spatial pattern between the observations and GCM historical simulations, with low thresholds in Northern Hemisphere (NH) high latitudes, central Asia, western United States, and high values in the southeastern United States, along the west coast of North America and in East Asia (Figs. ES4a,b). However, the average 99th-percentile threshold is very low and even zero in several grid cells in dry regions (e.g., Sahara) for some

models (Fig. ES4b). Most GCMs have a threshold smaller than 10 mm day^{-1} (which is often used as threshold to measure "heavy precipitation days"; Zhang et al. 2011) in such dry regions (Fig. ES4c). These low 99th-percentile thresholds may be less relevant in terms of "extremes" and small absolute changes may cause large relative changes. Therefore, to test the robustness of our results, we supplement additional analyses by excluding grid cells with low threshold (i.e., the 99th-percentile threshold < 10 mm) from the regional change analysis for observations (Fig. ES5). Similarly, grid cells with at least half of all models having such low threshold are also excluded from the regional change analysis and models having such low threshold are excluded from the gridcell change analysis (Fig. ES6). The conclusions still hold when excluding grid cells with threshold smaller than 10 mm (see, Fig. ES5 for observations and Fig. ES6 for GCM simulations).

Several past EPCD events (e.g., Tsuguti et al. 2019; Ulbrich et al. 2003; Webster et al. 2011) occurred in regions of complex orography, and it is possible that orographic effects play a role in the occurrence of such events. Therefore, we also use 22 regional climate models (RCM) from CORDEX (Giorgi et al. 2009) to verify if the results are sensitive to the representation of the underlying topography using RCM simulations for Europe and North America (Table ES2). We calculate the 99th percentile of all day precipitation of the observations, the RCM simulations, and the GCM simulations for Europe and North America (Figs. ES7a–f) and discuss the changes in the frequency for the RCM simulations (Figs. ES7g–j).

Definition of extreme precipitation on consecutive days. We identify extreme precipitation events when daily precipitation amounts exceed the 99th percentile of daily precipitation. The percentile is calculated based on all days, to avoid potential issues related to changes in wet-day frequency when calculating the percentile based on only wet days (Schär et al. 2016). We use the entire data period (1961–2010) as base period when calculating the percentile. In addition, to ensure robustness of our results to percentile level choice, we also tested other thresholds ranging from the 95th to the 99.9th percentile of all-day precipitation to identify daily extreme precipitation and analyze the changes in observed extreme precipitation on consecutive days (Fig. ES3), as the changes may be sensitive to the specific choice of threshold value (Pendergrass 2018). Daily extreme precipitation that exceeds the threshold for two or more consecutive days is defined as EPCD. Based on this definition, EPCD events can include both, temporally persistent events with a duration of two or more days or a temporal clustering of several individual events within a few days (e.g., Barton et al. 2016; Zscheischler et al. 2020). Both types of events represent potential hazards and are therefore included in this study based on the condition that extreme precipitation occurs on several consecutive days. We first calculate the frequency of EPCD for all stations. Then we interpolate the annual or seasonal results of all stations on a regular grid of 2° × 2° horizontal resolution using a bilinear interpolation algorithm. Grid cells containing no station are set as Nan value. We note that also two (or more) extreme precipitation days separated by one nonextreme day could result in a hazard, and our conclusions remain valid when modifying the definition to accommodate also this type of event (see, Fig. ES8).

Calculation of changes in EPCD frequency. Temporal changes in the observational time series at individual grid cells or regional averages are calculated using the ordinary least squares method, and trend significance is estimated using the Mann–Kendall test (Kendall 1955). The regional-mean time series are first normalized by the respective means in 1961–2010 before estimating the linear trend. Although the regional-mean time series representing continental-scale averages or latitude bands show roughly linear changes for the observations (Fig. 1b), we note that a linear trend is not necessarily the best fit to describe temporal changes in precipitation. Therefore, we also consider time-slice differences between the averages of

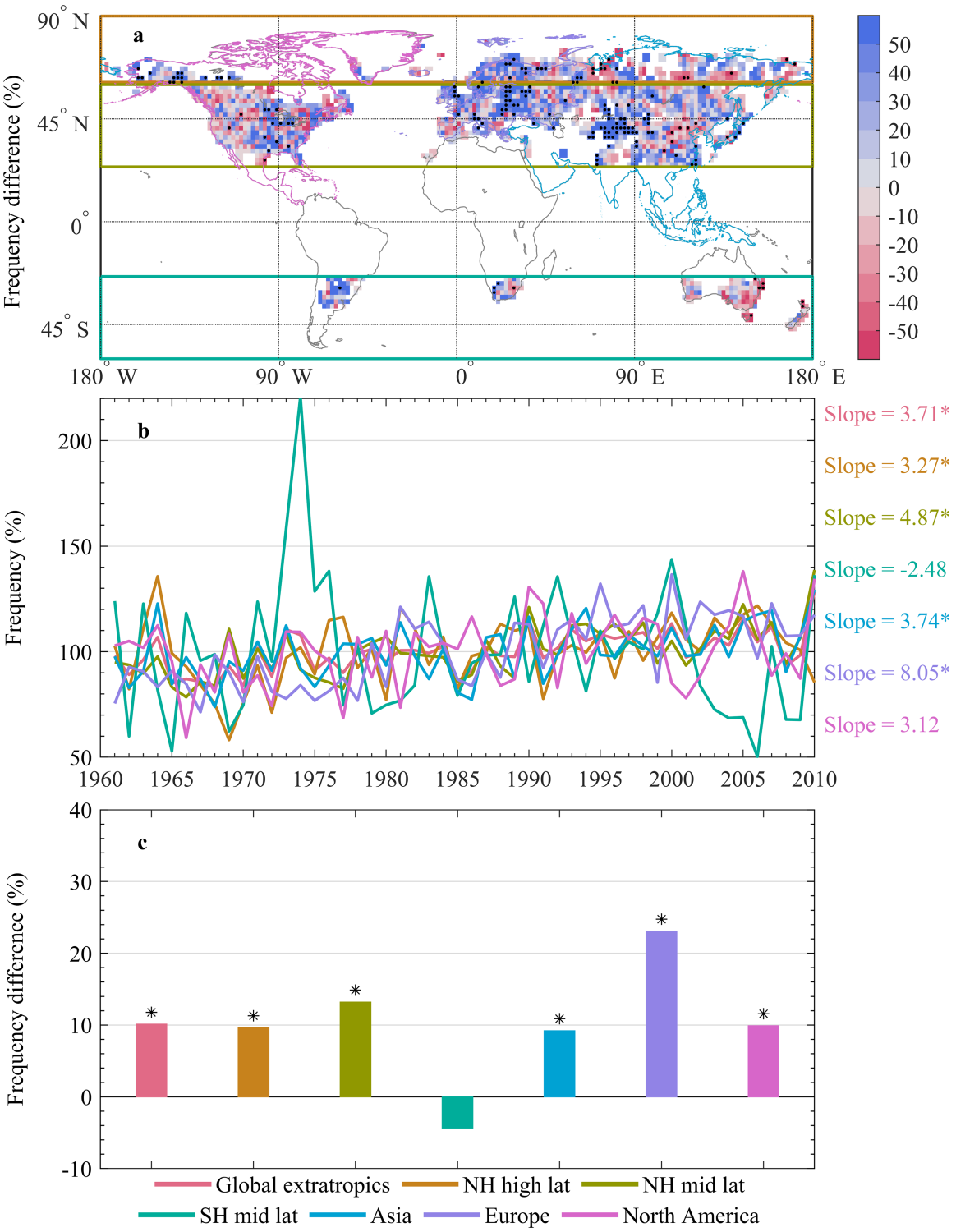

Fig. 1. Changes in the frequency of extreme precipitation on consecutive days identified from observations in 1961–2010. (a) Local changes (%) in mean frequency between 1961–85 and 1986–2010. (b) Hemispheric and continental average time series in 1961–2010. The annual frequency is normalized by the mean in 1961–2010. Slope (% decade^{-1}) is the linear trend by the ordinary least squares method. (c) Changes (%) in regional mean between both periods. The difference is a relative frequency change (see "Materials and methods" section). The stippling in (a) and the asterisks in (b) and (c) indicate a significant change ($p \leq 0.05$) according to the Wilcoxon rank sum test in (a) and (c) and the Mann–Kendall test in (b). The colored boxes or outlines in (a) define the regions for calculating the regional averages as presented by lines or bars of the corresponding colors in (b) and (c).

different periods for both observational and CMIP5 ensemble-mean time series. For each grid cell or regional averages, the differences for EPCD frequency, precipitation intensity (explained below), and autocorrelation (explained below) between two periods (1961–85 and 1986–2010 for observations and historical simulations, and 1961–2010 and 2071–100 for future projections) are defined as

$$D = \left(V_2 - V_1\right) \Big/ V_1 \times 100, \tag{1}$$

where D is the relative difference between both periods; V_1 and V_2 are the mean EPCD frequency/precipitation intensity during the earlier and later periods, respectively. The significance of local- and regional-mean changes between two periods is estimated by the Wilcoxon rank sum test. For historical and future simulations, we also consider the agreement of changes across models, i.e., the gridcell-level and regional changes are considered as "robust change" when more than 50% of the models show significant ($p \le 0.05$) change and at least 80% of models agree on the sign of change (Tebaldi et al. 2011).

Potential driving factors of the changes in EPCD frequency. Changes in EPCD frequency can be driven by multiple factors. On the one hand, they may be a consequence simply of changes in precipitation intensity, e.g., if precipitation intensifies there will be more days exceeding the threshold, and this increased number of daily extremes also increases the probability that the threshold is exceeded on consecutive days. On the other hand, also changes in the temporal correlation of daily extreme precipitation may result in daily extremes occurring more or less frequently on consecutive days, which would affect the frequency of EPCD. Therefore, we analyze whether the changes in EPCD frequency are related to changes in precipitation intensity and/or the temporal correlation of daily extreme precipitation time series.

We use the 99th percentile (P99) to represent precipitation intensity relevant to the analysis of EPCD frequency. To disentangle the effect of P99 changes on the changes in EPCD frequency, we use an adjusted threshold (i.e., the 99th-percentile threshold specifically for the first and second periods) to calculate the EPCD frequency, to ensure daily extremes exceeding the threshold occur on exactly 1% of the days in both periods (1961–85 and 1986–2010 for observations and historical simulations, and 1961–2010 and 2071–2100 for the future projections). We analyze the EPCD frequency changes 1) using a fixed threshold during 1961–2010 for both periods for observations (and 1961–2100 accordingly for the future projections) and 2) using the adjusted thresholds specific for the 1961–85 and 1986–2010 periods for observations (and 1961–2010 and 2071–2100 accordingly for the future projections) so that there are exactly 1% daily exceedances in each period. Approach 2 removes effects from possible intensity changes, and the remaining EPCD frequency changes in approach 2 (mean frequency in 1986–2010 minus frequency in 1961–85) are therefore attributable to other factors such as temporal correlation (F_{ac}) of daily extreme precipitation. The EPCD frequency changes between both periods in approach 1 are due to potential changes in both intensity and temporal correlation. The difference between these two approaches (the remaining change between both periods in approach 1 minus that in approach 2) is considered as the effect related to intensity changes (F_{P99}).

We use the first-order autocorrelation (AC) of the occurrence daily extreme precipitation to characterize changes in the temporal correlation of extreme precipitation (exceeding P99), rather than the AC of daily extreme precipitation amount, which avoids the effects of precipitation intensity on the autocorrelation. This requires transferring the daily precipitation series to binary data (0–1 data, where "0" represents nonextreme day and "1" days with extreme precipitation). We then use the Matthews correlation coefficient, which was originally developed by Matthews (1975) and reproposed by Baldi et al. (2000), to calculate the AC based on

all 0–1 data (where extremes are identified against the adjusted percentile threshold for the two periods, to avoid effects from changing frequency of extremes and indeed quantify the temporal sequencing). The Matthews correlation coefficient is suited to binary data, and can effectively overcome the class imbalance issue (i.e., the number of samples in one class (e.g., "0") is much larger than the number of samples in another class (e.g., "1") for 0–1 binary data (Chicco and Jurman 2020; Chicco et al. 2021). The change of AC between two periods is the difference of the AC during the later period minus the AC during the earlier period. An increase in AC indicates that extreme precipitation events tend to occur more often on consecutive days and a decrease that they occur more often as part of temporally separated single-day events. Similar to the calculation of EPCD frequency, intensity and temporal correlation of daily precipitation events are first calculated for each station before being interpolated onto a 2° × 2° grid.

We calculate the relative contribution of changes in precipitation intensity and temporal correlation on EPCD frequency changes by separating the effects of both factors on the changes in EPCD frequency shown as F_{ac} and F_{P99} above. The relative contribution of precipitation intensity (C_{P99}) is calculated as

$$C_{P99} = \left|F_{P99}\right| \Big/ \left(\left|F_{P99}\right| + \left|F_{ac}\right|\right) \times 100, \tag{2}$$

where |*| represents the absolute value of "*." The absolute values of F_{P99} and F_{ac} are used to avoid a contribution larger than 100% in the case of F_{P99} or F_{ac} being negative numbers. Similarly, the relative contribution of changes in the temporal correlation of extreme precipitation (C_{ac}) is calculated as

$$C_{ac} = \left|F_{ac}\right| \Big/ \left(\left|F_{P99}\right| + \left|F_{ac}\right|\right) \times 100. \tag{3}$$

Results

Changes in the frequency of extreme precipitation on consecutive days. The observed EPCD events have become more frequent for large regions of the global extratropics, especially in Europe (Fig. 1a). Despite some spatial heterogeneity in the change patterns, there are larger areas showing increases than showing decreases. At continental scales, Europe has the largest upward trend in the frequency of EPCD by 8.05% decade^{-1} ($p \le 0.05$, Fig. 1b), or increases by 23.1% between the averages of the two periods 1961–85 and 1986–2010 (Fig. 1c). Besides Europe, the NH midlatitudes in general exhibit a strong increase in area-averaged EPCD frequency, which may be dominated by the large increase in Europe (Fig. 1a). Other regions also show significant ($p \le 0.05$) upward trends in EPCD frequency, except Southern Hemisphere (SH) midlatitudes, which are characterized by the notable decreases in South Africa, southern Australia, and New Zealand. This is consistent with the decreasing trend in precipitation event duration and the significant decreases in the frequency of precipitation events with durations of more than two days in southern Australia (Dey et al. 2020). We also note that there is a strong peak in mid-1970s in the regional frequency time series of SH midlatitudes (Fig. 1b). These strong anomalies occur mainly in eastern Australia (Fig. ES9), coinciding with the strong 1973/74 La Niña event, which has been associated with widespread and severe flooding in eastern Australia (National Climate Centre 2011).

Complementing the observational results with analyses of climate model simulations, providing complete spatial coverage, we find that EPCD frequency derived from the CMIP5 ensemble during the observational periods (1961–85 and 1986–2010) shows predominantly EPCD increases (although generally not significant at gridcell level) in large parts of global land areas (Fig. 2a). These simulated (ensemble-mean) increases are more homogeneous compared

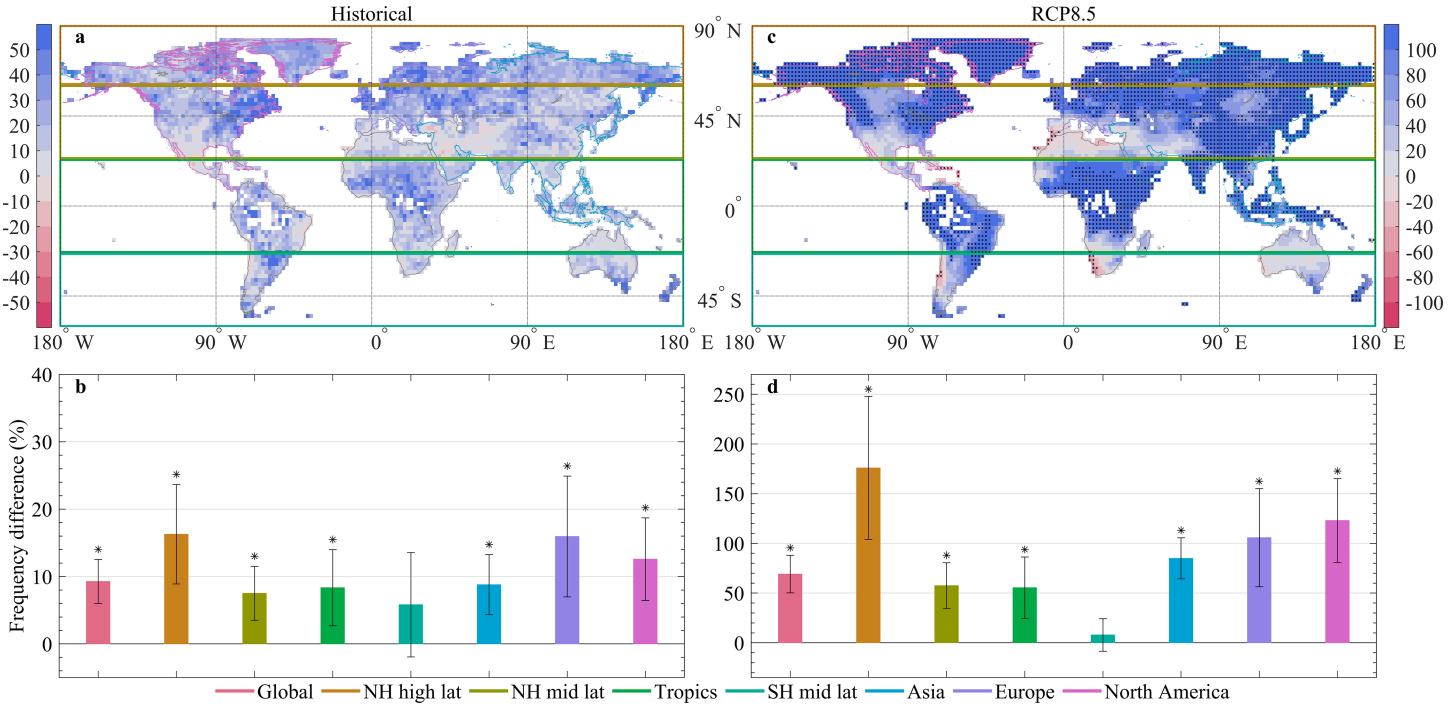

Fig. 2. Changes in the frequency of extreme precipitation on consecutive days for historical and future simulations. (a),(c) Local changes (%) (left) between 1961–85 and 1986–2010 for historical simulations and (right) between 1961–2010 and 2071–2100 for RCP8.5 scenario identified from the ensemble mean of the CMIP5 simulations. We merge the historical (1961–2005) and RCP8.5 (2006–10) simulations to have the CMIP5 past data over exactly the same period as observations, i.e., data for 1961–2010 (see "Materials and methods" section). (b),(d) The corresponding regional average changes (%) in (a) and (c). The difference is a relative frequency change between both periods (see "Materials and methods" section). Stippling in (a) and (c) and asterisks in (b) and (d) indicate "robust change" across all models (see "Materials and methods" section). Error bars in (b) and (d) represents plus and minue one ensemble standard deviation. Colored regions (except tropics) are as in Fig. 1. Note that the *y*-axis scale is different between observations, historical simulations, and future projections.

to the observed changes, where some regions like northern Siberia exhibit robust decreases in observations, by contrast to the model simulations. For the different regional averages, the EPCD frequency changes are significant ($p \leq 0.05$) for NH mid- and high-latitude regions (Fig. 2b). Similar to the observational results, the simulated increase in EPCD frequency between both periods is large in Europe. Also, a relatively weak and nonsignificant ($p > 0.05$) change in EPCD frequency over the past 50 years is found in the SH midlatitudes. The results of the regional changes in EPCD frequency for the historical simulations also still hold when using the spatial coverage mask of the observations (Fig. ES10).

Future projections from the CMIP5 multimodel ensemble also show significant increases ($p \leq 0.05$) in EPCD frequency between 1961–2010 and 2071–2100 in most global land areas (except the Mediterranean region, northern Latin America, and large parts of the SH midlatitudes) for the RCP8.5 scenario (Fig. 2c). Europe, NH high latitudes, Asia, and North America show the strongest increases, whereas the SH midlatitudes average shows a nonsignificant ($p > 0.05$) change (Fig. 2d). The projected EPCD frequency changes are similar in sign to (although stronger than) changes found in the observations (Fig. 1c) and historical simulations (Fig. 2b), and changes are larger under stronger radiative forcing (cf. RCP8.5, Fig. 2d, and RCP4.5, Fig. ES11). These similarities suggest that observed changes in EPCD frequency are consistent with a warming climate and therefore expected to continue with further warming.

The observed changes in the seasonal frequency of EPCD are mostly similar to the annual changes (Fig. ES12 versus Fig. 1). In particular the EPCD increases in Europe and the NH high latitudes are strongest during boreal spring (March–May) and summer (June–August). Also the SH midlatitudes show significant increases during austral spring (September–November), while the other seasons show decreases or no changes. Also, the projected future changes in

seasonal EPCD frequency are mostly similar to the annual changes for the RCP8.5 scenario (Fig. ES13 versus Figs. 2c,d). Significant EPCD increases are projected for most NH midlatitude and high-latitude regions in all seasons, and the magnitude of projected increases is largest in boreal spring, autumn (September–November), and winter (December–February) (Fig. ES13).

The CMIP5 GCM simulations may have a poor representation of the underlying topography and related effects due to their relatively coarse horizontal resolution. Therefore, we also use RCMs with higher horizontal resolution to verify if the results are sensitive to the representation of the underlying topography for Europe and North America. Although the spatial gradients of threshold are weaker in the RCMs compared to observations, results show a similar spatial pattern between the observations and RCM simulations (e.g., highest 99th-percentile values in the southeastern United States, along the west coast of North America and in the Alps) (Figs. ES7a–f). In particular the RCM-based spatial patterns are more similar to observations than the GCM-based patterns, which largely miss the observed gradients. The RCM-simulated changes confirm the widespread EPCD increases over large areas of North America and Europe, similar to the GCM results and observations (Figs. ES7g–j).

Effects of rainfall intensification and temporal autocorrelation changes on the changes in EPCD frequency. To better understand the contributions from the different drivers of the changes in EPCD frequency, we isolate the effects of intensity changes on EPCD frequency, by using an adjusted 99th-percentile threshold specific for each period, to ensure the threshold exceedance probability is equal in both periods (see "Materials and methods" section). This analysis shows considerably weaker (and fewer) regional increases of EPCD frequency in both observations (Figs. 3a,b) and model simulations (Figs. 4a,b). This indicates that most of these regional EPCD frequency changes are primarily a consequence of changes in precipitation intensity, especially for NH high latitudes, North America, and Asia. However, a larger area in central Europe and NH midlatitudes remains where observed EPCD frequency increases (locally not significant, but spatially aggregated over Europe and the NH midlatitudes a significant EPCD increase remains) after removing the effects of intensity changes (Fig. 3a). These areas correspond to regions of increased autocorrelation of daily extremes (AC) (Fig. 3c), suggesting that changes in the temporal correlation (see "Materials and methods" section) of extreme precipitation also play a role here. Seasonal analysis also shows a significant increase ($p \leq 0.05$) of the EPCD frequency in particular in spring in the NH mid- and high latitudes, Asia, and North America (Fig. ES14a) after removing the effects of intensity changes. This is consistent with the significantly ($p \leq 0.05$) increased AC of daily extreme precipitation in particular in NH high and midlatitudes and North America (Fig. ES14e). Moreover, AC also significantly increases in Europe in summer (Fig. ES14f), which contributes to the observed significant increase ($p \leq 0.05$) in EPCD frequency (Fig. ES14b). For SH midlatitudes, the adjusted summer (DJF) EPCD frequency decreases (–14.1%) after removing the effects of intensity changes (Fig. ES14d), which is consistent with the significant ($p \leq 0.05$) decrease in AC (Fig. ES14h). This indicates that the observed lack of increase in the EPCD frequency in SH midlatitudes (Fig. 1) is mainly attributed to the change in austral summer, and that the decreasing AC dominates the decrease in frequency. These results suggest that changes in temporal correlation of daily extreme precipitation play an important role in decreasing EPCD frequency in the SH midlatitudes and amplifying it in Europe, for example.

Future climate projections confirm that changes in precipitation AC locally counteract or amplify the EPCD increases expected from rainfall intensification. The spatial distribution of the sign of changes in EPCD frequency after removing the effects of intensity changes is in general very similar to that of the change signs in AC (Figs. 4a,c). In most of the NH high latitudes, northern North America, parts of central Asia and Africa, decreasing AC is projected (Fig. 4c), where the adjusted EPCD frequency is projected to decrease (Fig. 4a)

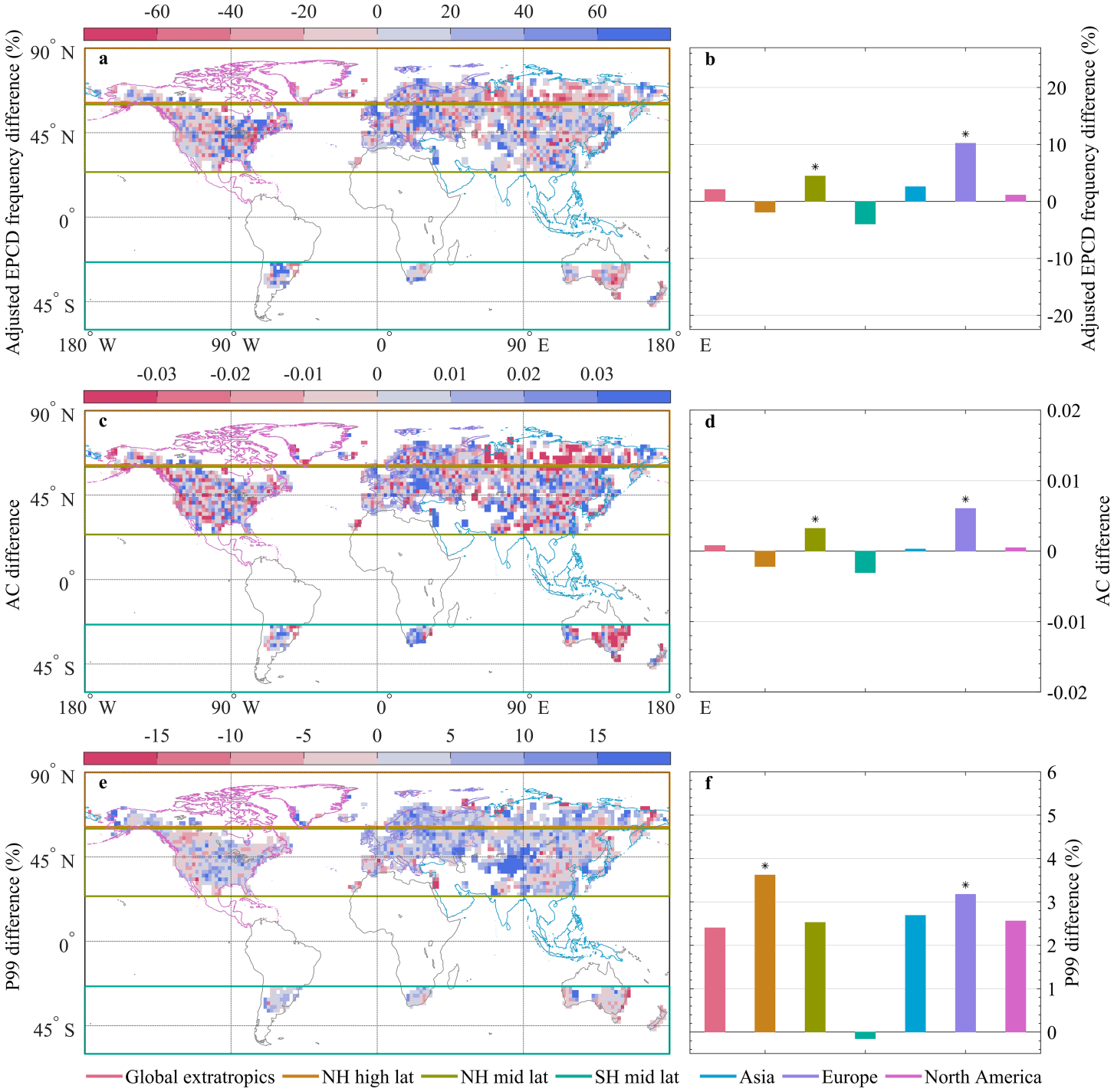

Fig. 3. Local and regional changes in adjusted frequency of extreme precipitation on consecutive days, autocorrelation, and precipitation intensity between 1961–85 and 1986–2010 for observations. (a),(b) EPCD frequency changes (%) after removing the effects of possible intensity changes (see "Materials and methods" section). (c),(d) Changes in autocorrelation in the daily extreme precipitation time series. (e),(f) Changes (%) daily intensity of precipitation for the 99th percentile of all-day precipitation. Asterisks in (b), (d), and (f) indicate a significant change estimated by the Wilcoxon rank sum test. Colored regions are as in Fig. 1.

(and significantly decrease in regional average for the NH high latitudes and North America, Fig. 4b) while the EPCD frequency is projected to significantly increase (Fig. 2c), consistent with the increasing intensity of extreme precipitation (P99, Figs. 4e,f). This indicates the changes in EPCD frequency are affected by changes in the temporal correlation of extreme precipitation reducing the effects of intensity changes in these regions for the RCP8.5 scenario.

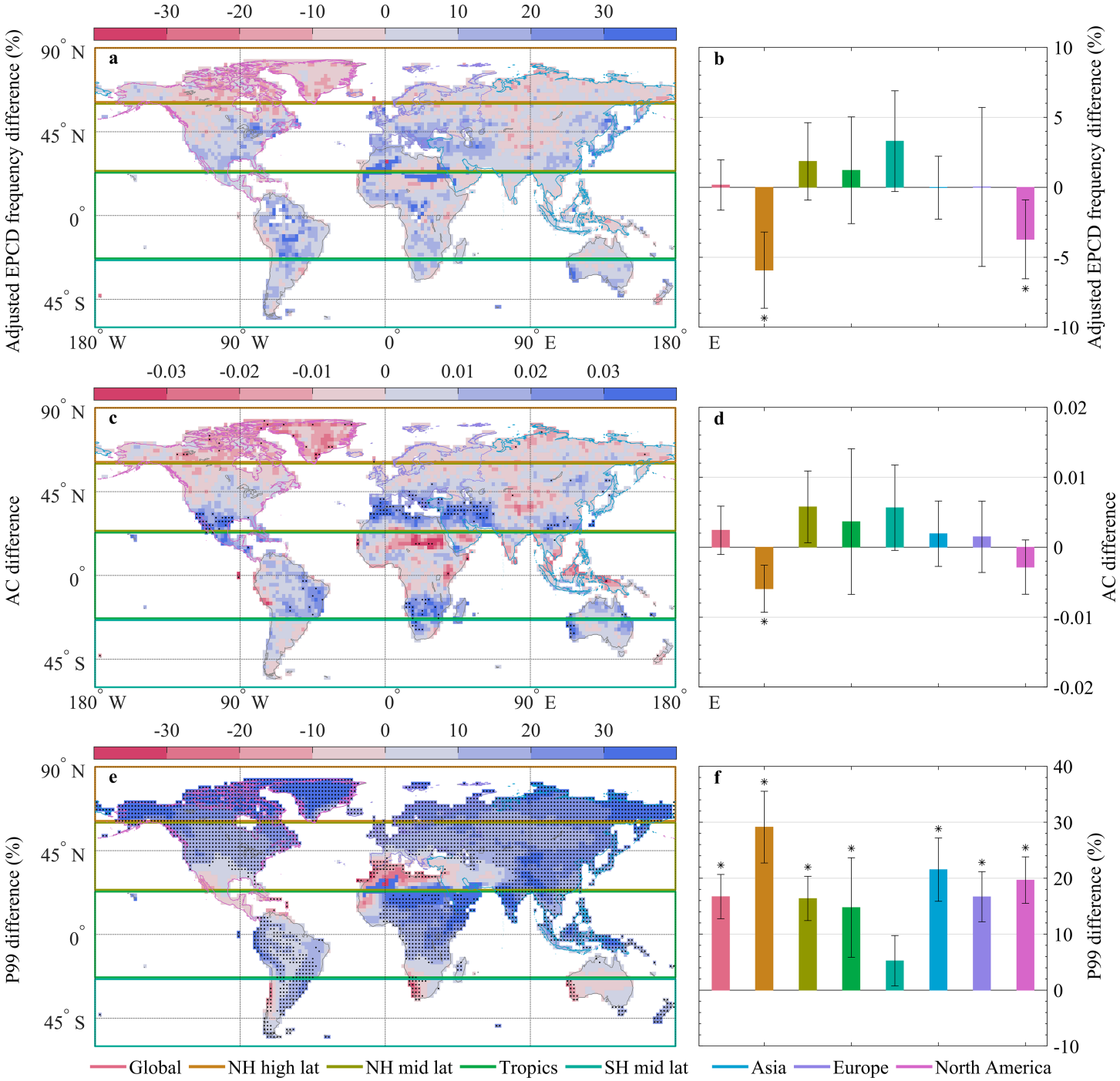

Fig. 4. Changes in adjusted frequency of extreme precipitation on consecutive days, autocorrelation, and precipitation intensity between 1961–2010 and 2071–2100 for historical + RCP8.5 scenario simulations. (a),(b) EPCD frequency changes (%) after removing the effects of possible intensity changes. (c),(d) Changes in autocorrelation in the daily extreme precipitation time series. (e),(f) Changes (%) in daily intensity of precipitation for the 99th percentile of all-day precipitation. Stippling in (a) and asterisks in (b), (d), and (f) indicate "robust change" across all models (see "Materials and methods" section). Stippling in (c) and (e) represents that at least 80% of models agree on the change sign. Error bars in (b), (d), and (f) represent plus and minus one ensemble standard deviation.

For larger regional averages, although changes in the temporal correlation of extreme precipitation play a role in driving the changes in EPCD frequency in some regions, increased precipitation intensity (Fig. 4f) causes more EPCD frequency increases (Fig. 2d) compared to the effects of the changes in temporal correlation (Fig. 4b). Therefore, the increasing EPCD frequency in future climate projections (Figs. 2c,d) is primarily a consequence of increased precipitation intensity for most regions. Similar results are found for the RCP4.5 scenario (Fig. ES15).

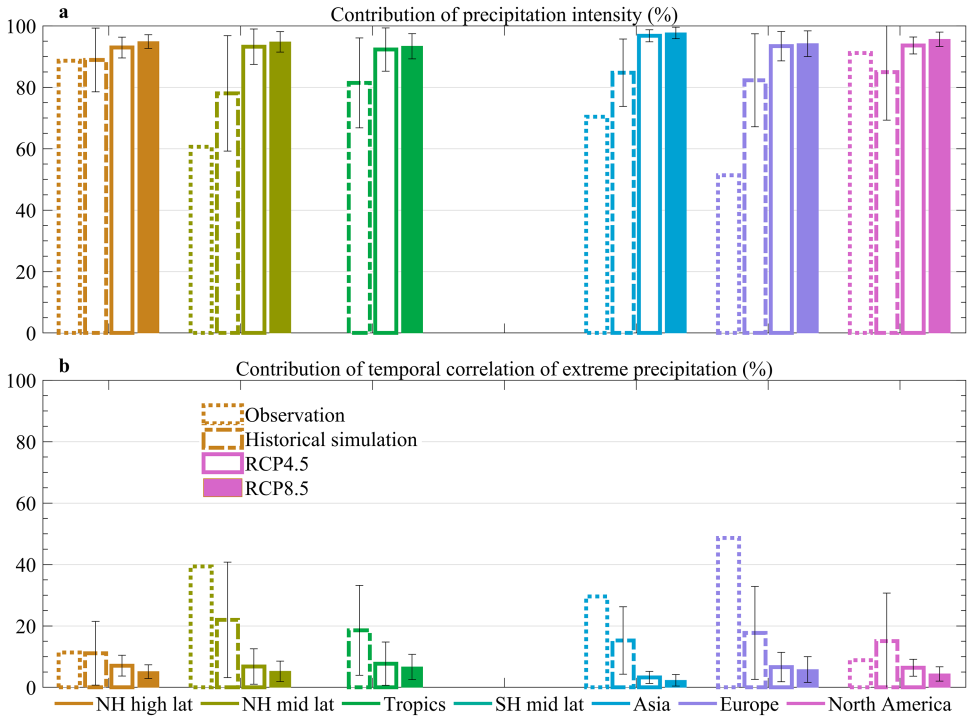

Fig. 5. Contribution of regional changes in the temporal correlation of extreme precipitation and precipitation intensity on regional changes to the frequency of extreme precipitation on consecutive days. (a) Precipitation intensity–related contribution for observations (the first bar in each region class), historical simulations (the second bar), and future projections (RCP4.5 and RCP8.5 in the third and fourth bar, respectively). (b) Temporal correlation of extreme precipitation related contribution. Error bars represent plus and minus one ensemble standard deviation. Definition of the contribution is shown in the "Materials and methods" section. The contribution is calculated only when the change in regional-mean frequency is significant ($p \leq 0.05$); otherwise, the contribution values are set to zero.

Relative contribution of P99 and AC changes on the changes in EPCD frequency. The observed and simulated EPCD frequency changes are a consequence of the combined effects of changing temporal correlation of extreme precipitation and intensity. The changes in temporal correlation of extreme precipitation can reduce or amplify the increases in EPCD frequency expected from precipitation intensification alone. Overall, precipitation intensity increases for large areas of the globe and contributes on average 80%–90% to EPCD frequency increases in most regions (Fig. 5a). Both positive and negative contributions of temporal correlation changes account for on average 10%–20% (Fig. 5b) of the EPCD frequency changes. However, the relative contribution of future precipitation intensification will become stronger and the contribution of future temporal correlation changes relatively weaker with increased global warming, compared with the historical simulation. For example, the relative contribution of the precipitation intensification increases from ~80% for historical simulation to ~95% for the future RCP8.5 scenario projections in Europe.

Summary

This study shows that in most regions of the NH extratropics, and especially in Europe, EPCD events have been significantly increasing in frequency during the last half century, using a unique quasi-global collection of daily in situ data from 6,006 stations. The EPCD frequency is projected to further increase for most regional means (except SH midlatitudes) in the model simulations under increasing radiative forcing, in agreement with previous finding of consistently intensifying trends for precipitation extremes at a global-average scale (Kao and Ganguly 2011) and increases in clustering in the occurrence of precipitation extremes (Tuel

and Martius 2021). Increases in both temporal autocorrelation of extreme precipitation and intensity have positive contributions to EPCD frequency increases, e.g., in the NH midlatitudes and Europe. In fact, Europe has been affected by several precipitation events that persisted over several days in recent decades and led to severe flooding (Kundzewicz et al. 2005; Ulbrich et al. 2003). However, the differences in the magnitude and signs of both variables result in regionally different EPCD frequency changes. Decreases in future extreme precipitation temporal autocorrelation projected in NH high latitudes, central Asia, Southeast Asia, and central Africa counteract the effects from intensification of the hydrologic cycle (DeAngelis et al. 2015; Giorgi et al. 2011; Wu et al. 2013) and thereby explain the regionally smaller increases in EPCD frequency with warming than expected from intensification alone. For other regions, however, increased temporal correlation of extreme precipitation may enhance the intensity-related increased EPCD frequency. In particular in the NH midlatitudes, North America, and Europe the observed increasing autocorrelation of daily extreme precipitation in boreal spring and summer appears consistent with previous studies indicating a tendency toward more persistent atmospheric circulation patterns (Mann et al. 2017). Especially, the significantly increased average AC in Europe in summer may be related to the previously reported more stationary circulation in summer affecting Europe (Kornhuber et al. 2017; Wolf et al. 2018) and thus contributes to the observed significant increase ($p \leq 0.05$) in EPCD frequency. Also, the dry subtropics all generally show robust increases in AC. That may be related to a relative narrowing of the wet season or to changes in atmospheric stability that make extreme precipitation less likely on average, so that extremes will tend to follow each other when the right conditions are met (Pfahl et al. 2017). Although the changes in temporal correlation play an important role affecting the EPCD in some regions (e.g., the contribution of temporal correlation to the observed increasing EPCD frequency even reaches at 50% in Europe), precipitation intensity increases dominate the EPCD frequency increases in most regions in particular for the future RCP8.5 scenario projections. Moreover, the contribution of precipitation intensification to the increase in EPCD frequency is projected to increase with future climate warming. While flooding is affected by a number of factors, and a link between changes in extreme precipitation intensity and flooding is not clearly observed (Sharma et al. 2018), extreme precipitation occurring on consecutive days affects e.g., soil preconditioning and thereby is likely an important factor in increasing flood risk (Wasko and Nathan 2019). Therefore, our results also indicate that more attention should be paid to Europe, United States, East Asia, and NH midlatitudes, where the interaction of changing temporal correlation of extreme precipitation and increasing intensity indicate largest increases in extreme precipitation events on consecutive days, potentially increasing the risk of severe river flooding.

Acknowledgments. We acknowledge support from the National Key R&D Program of China (2019YFC0409101), Science and Technology Development Plan of Jilin Province (20190201291JC), the Joint Fund of National Natural Science Foundation of China (U19A2023), the Fundamental Research Funds for the Central Universities (2412020FZ002), and 2236 Co-Funded Brain Circulation Scheme2 (CoCirculation2) of TÜBİTAK (121C054). M.G.D. acknowledges support by the Horizon 2020 EUCP project under Grant Agreement 776613 and by the Spanish Ministry for the Economy, Industry and Competitiveness Ramón y Cajal 2017 Grant Reference RYC-2017-22964.

Data availability statement. The following data are available online: the CMIP5 GCM simulations (http://pcmdi9.llnl.gov/), the CORDEX RCM simulations (www.cordex.org/), the GHCND dataset (www.ncdc.noaa.gov/ghcn-daily-description), the ECA&D dataset (www.ecad.eu/), the USHCN dataset (http://cdiac.ess-dive.lbl.gov/ftp/ushcn_daily/), and the data in Canada (http://climate.weather.gc.ca/). Seasonal and annual EPCD frequency, adjusted EPCD frequency, AC, and P99 for observations are available at http://doi.org/10.5281/zenodo.4835733.

References

Alexander, L. V., and Coauthors, 2006: Global observed changes in daily climate extremes of temperature and precipitation. *J. Geophys. Res.*, **111**, D05109, https://doi.org/10.1029/2005JD006290.

Allen, M. R., and W. J. Ingram, 2002: Constraints on future changes in climate and the hydrologic cycle. *Nature*, **419**, 228–232, https://doi.org/10.1038/nature01092.

Asadieh, B., and N. Krakauer, 2015: Global trends in extreme precipitation: Climate models versus observations. *Hydrol. Earth Syst. Sci.*, **19**, 877–891, https://doi.org/10.5194/hess-19-877-2015.

Baldi, P., S. Brunak, Y. Chauvin, C. A. Andersen, and H. Nielsen, 2000: Assessing the accuracy of prediction algorithms for classification: An overview. *Bioinformatics*, **16**, 412–424, https://doi.org/10.1093/bioinformatics/16.5.412.

Barbero, R., H. J. Fowler, G. Lenderink, and S. Blenkinsop, 2017: Is the intensification of precipitation extremes with global warming better detected at hourly than daily resolutions? *Geophys. Res. Lett.*, **44**, 974–983, https://doi.org/10.1002/2016GL071917.

Barton, Y., P. Giannakaki, H. Von Waldow, C. Chevalier, S. Pfahl, and O. Martius, 2016: Clustering of regional-scale extreme precipitation events in southern Switzerland. *Mon. Wea. Rev.*, **144**, 347–369, https://doi.org/10.1175/MWR-D-15-0205.1.

Chicco, D., and G. Jurman, 2020: The advantages of the Matthews correlation coefficient (MCC) over F1 score and accuracy in binary classification evaluation. *BMC Genomics*, **21**, 6, https://doi.org/10.1186/s12864-019-6413-7.

——, T. Niklas, and G. Jurman, 2021: The Matthews correlation coefficient (MCC) is more reliable than balanced accuracy, bookmaker informedness, and markedness in two-class confusion matrix evaluation. *BioData Min.*, **14**, 13, https://doi.org/10.1186/s13040-021-00244-z.

DeAngelis, A. M., X. Qu, M. D. Zelinka, and A. Hall, 2015: An observational radiative constraint on hydrologic cycle intensification. *Nature*, **528**, 249–253, https://doi.org/10.1038/nature15770.

Dey, R., A. J. E. Gallant, and S. C. Lewis, 2020: Evidence of a continent-wide shift of episodic rainfall in Australia. *Wea. Climate Extremes*, **29**, 100274, https://doi.org/10.1016/j.wace.2020.100274.

Donat, M. G., and Coauthors, 2013: Updated analyses of temperature and precipitation extreme indices since the beginning of the twentieth century: The HadEX2 dataset. *J. Geophys. Res. Atmos.*, **118**, 2098–2118, https://doi.org/10.1002/jgrd.50150.

——, A. L. Lowry, L. V. Alexander, P. A. O'Gorman, and N. Maher, 2016: More extreme precipitation in the world's dry and wet regions. *Nat. Climate Change*, **6**, 508–513, https://doi.org/10.1038/nclimate2941.

Du, H., Z. Wu, S. Zong, X. Meng, and L. Wang, 2013: Assessing the characteristics of extreme precipitation over northeast China using the multifractal detrended fluctuation analysis. *J. Geophys. Res. Atmos.*, **118**, 6165–6174, https://doi.org/10.1002/jgrd.50487.

Dwyer, J. G., and P. A. O'Gorman, 2017: Changing duration and spatial extent of midlatitude precipitation extremes across different climates. *Geophys. Res. Lett.*, **44**, 5863–5871, https://doi.org/10.1002/2017GL072855.

Fischer, E. M., and R. Knutti, 2015: Anthropogenic contribution to global occurrence of heavy-precipitation and high-temperature extremes. *Nat. Climate Change*, **5**, 560–564, https://doi.org/10.1038/nclimate2617.

Giorgi, F., C. Jones, and G. R. Asrar, 2009: Addressing climate information needs at the regional level: The CORDEX Framework. *WMO Bull.*, **58**, 175–183.

——, E. S. Im, E. Coppola, N. S. Diffenbaugh, X. J. Gao, L. Mariotti, and Y. Shi, 2011: Higher hydroclimatic intensity with global warming. *J. Climate*, **24**, 5309–5324, https://doi.org/10.1175/2011JCLI3979.1.

Guerreiro, S. B., H. J. Fowler, R. Barbero, S. Westra, G. Lenderink, S. Blenkinsop, E. Lewis, and X.-F. Li, 2018: Detection of continental-scale intensification of hourly rainfall extremes. *Nat. Climate Change*, **8**, 803–807, https://doi.org/10.1038/s41558-018-0245-3.

Guilbert, J., A. K. Betts, D. M. Rizzo, B. Beckage, and A. Bomblies, 2015: Characterization of increased persistence and intensity of precipitation in the northeastern United States. *Geophys. Res. Lett.*, **42**, 1888–1893, https://doi.org/10.1002/2015GL063124.

Kao, S. C., and A. R. Ganguly, 2011: Intensity, duration, and frequency of precipitation extremes under 21st-century warming scenarios. *J. Geophys. Res.*, **116**, D16119, https://doi.org/10.1029/2010JD015529.

Kendall, M. G., 1955: *Rank Correlation Methods.* Hafner Publishing Co., 196 pp.

Klein Tank, A. M. G., and Coauthors, 2002: Daily dataset of 20th-century surface air temperature and precipitation series for the European Climate Assessment. *Int. J. Climatol.*, **22**, 1441–1453, https://doi.org/10.1002/joc.773.

Kornhuber, K., V. Petoukhov, S. Petri, S. Rahmstorf, and D. Coumou, 2017: Evidence for wave resonance as a key mechanism for generating high-amplitude quasi-stationary waves in boreal summer. *Climate Dyn.*, **49**, 1961–1979, https://doi.org/10.1007/s00382-016-3399-6.

——, S. Osprey, D. Coumou, S. Petri, V. Petoukhov, S. Rahmstorf, and L. Gray, 2019: Extreme weather events in early summer 2018 connected by a recurrent hemispheric wave-7 pattern. *Environ. Res. Lett.*, **14**, 054002, https://doi.org/10.1088/1748-9326/ab13bf.

Kreienkamp, F., and Coauthors, 2021: Rapid attribution of heavy rainfall events leading to the severe flooding in western Europe during July 2021. World Weather Attribution Rep., 51 pp., http://hdl.handle.net/1854/LU-8732135.

Kundzewicz, Z. W., and Coauthors, 2005: Summer floods in central Europe—Climate change track? *Nat. Hazards*, **36**, 165–189, https://doi.org/10.1007/s11069-004-4547-6.

Mann, M. E., S. Rahmstorf, K. Kornhuber, B. A. Steinman, S. K. Miller, and D. Coumou, 2017: Influence of anthropogenic climate change on planetary wave resonance and extreme weather events. *Sci. Rep.*, **7**, 45 242, https://doi.org/10.1038/srep45242.

Matthews, B. W., 1975: Comparison of the predicted and observed secondary structure of T4 phage lysozyme. *Biochim. Biophys. Acta, Protein Struct.*, **405**, 442–451, https://doi.org/10.1016/0005-2795(75)90109-9.

Menne, M. J., I. Durre, R. S. Vose, B. E. Gleason, and T. G. Houston, 2012: An overview of the Global Historical Climatology Network-Daily database. *J. Atmos. Oceanic Technol.*, **29**, 897–910, https://doi.org/10.1175/JTECH-D-11-00103.1.

——, J. C. N. Williams, and R. S. Vose, 2016: Long-term daily and monthly climate records from stations across the contiguous United States. CDIAC, accessed 2 April 2016, https://doi.org/10.3334/CDIAC/CLI.NDP019.

National Climate Centre, 2011: Frequent heavy rain events in late 2010/early 2011 lead to widespread flooding across eastern Australia. Bureau of Meteorology Special Climate Statement 24, 28 pp.

O'Gorman, P. A., and T. Schneider, 2009: The physical basis for increases in precipitation extremes in simulations of 21st-century climate change. *Proc. Natl. Acad. Sci. USA*, **106**, 14 773–14 777, https://doi.org/10.1073/pnas.0907610106.

Pendergrass, A. G., 2018: What precipitation is extreme? *Science*, **360**, 1072–1073, https://doi.org/10.1126/science.aat1871.

Pfahl, S., P. A. O'Gorman, and E. M. Fischer, 2017: Understanding the regional pattern of projected future changes in extreme precipitation. *Nat. Climate Change*, **7**, 423–427, https://doi.org/10.1038/nclimate3287.

Pfleiderer, P., C.-F. Schleussner, K. Kornhuber, and D. Coumou, 2019: Summer weather becomes more persistent in a 2°C world. *Nat. Climate Change*, **9**, 666–671, https://doi.org/10.1038/s41558-019-0555-0.

Schär, C., and Coauthors, 2016: Percentile indices for assessing changes in heavy precipitation events. *Climatic Change*, **137**, 201–216, https://doi.org/10.1007/s10584-016-1669-2.

Screen, J. A., and I. Simmonds, 2014: Amplified mid-latitude planetary waves favour particular regional weather extremes. *Nat. Climate Change*, **4**, 704–709, https://doi.org/10.1038/nclimate2271.

Sharma, A., C. Wasko, and D. P. Lettenmaier, 2018: If precipitation extremes are increasing, why aren't floods? *Water Resour. Res.*, **54**, 8545–8551, https://doi.org/10.1029/2018WR023749.

Shepherd, T. G., 2014: Atmospheric circulation as a source of uncertainty in climate change projections. *Nat. Geosci.*, **7**, 703–708, https://doi.org/10.1038/ngeo2253.

Tebaldi, C., J. M. Arblaster, and R. Knutti, 2011: Mapping model agreement on future climate projections. *Geophys. Res. Lett.*, **38**, L23701, https://doi.org/10.1029/2011GL049863.

Trenberth, K. E., 2011: Changes in precipitation with climate change. *Climate Res.*, **47**, 123–138, https://doi.org/10.3354/cr00953.

Tsuguti, H., N. Seino, H. Kawase, Y. Imada, T. Nakaegawa, and I. Takayabu, 2019: Meteorological overview and mesoscale characteristics of the heavy rain event of July 2018 in Japan. *Landslides*, **16**, 363–371, https://doi.org/10.1007/s10346-018-1098-6.

Tuel, A., and O. Martius, 2021: A global perspective on the sub-seasonal clustering of precipitation extremes. *Wea. Climate Extremes*, **33**, 100348, https://doi.org/10.1016/j.wace.2021.100348.

Ulbrich, U., T. Brücher, A. H. Fink, G. C. Leckebusch, A. Krüger, and J. G. Pinto, 2003: The central European floods of August 2002: Part 1—Rainfall periods and flood development. *Weather*, **58**, 371–377, https://doi.org/10.1256/wea.61.03A.

Vincent, L. A., X. L. Wang, E. J. Milewska, H. Wan, F. Yang, and V. Swail, 2012: A second generation of homogenized Canadian monthly surface air temperature for climate trend analysis. *J. Geophys. Res.*, **117**, D18110, https://doi.org/10.1029/2012JD017859.

Wang, X. L., and Y. Feng, 2013: RhtestsV4 user manual. Environment Canada Science and Technology Branch Climate Research Division Doc., 29 pp., http://etccdi.pacificclimate.org/software.shtml.

Wasko, C., and R. Nathan, 2019: Influence of changes in rainfall and soil moisture on trends in flooding. *J. Hydrol.*, **575**, 432–441, https://doi.org/10.1016/j.jhydrol.2019.05.054.

Webster, P. J., V. E. Toma, and H.-M. Kim, 2011: Were the 2010 Pakistan floods predictable? *Geophys. Res. Lett.*, **38**, L04806, https://doi.org/10.1029/2010GL046346.

Westra, S., L. V. Alexander, and F. W. Zwiers, 2013: Global increasing trends in annual maximum daily precipitation. *J. Climate*, **26**, 3904–3918, https://doi.org/10.1175/JCLI-D-12-00502.1.

Wolf, G., D. J. Brayshaw, N. P. Klingaman, and A. Czaja, 2018: Quasi-stationary waves and their impact on European weather and extreme events. *Quart. J. Roy. Meteor. Soc.*, **144**, 2431–2448, https://doi.org/10.1002/qj.3310.

Wu, P., N. Christidis, and P. Stott, 2013: Anthropogenic impact on Earth's hydrological cycle. *Nat. Climate Change*, **3**, 807–810, https://doi.org/10.1038/nclimate1932.

Zhang, X., L. Alexander, G. C. Hegerl, P. Jones, A. K. Tank, T. C. Peterson, B. Trewin, and F. W. Zwiers, 2011: Indices for monitoring changes in extremes based on daily temperature and precipitation data. *Wiley Interdiscip. Rev.: Climate Change*, **2**, 851–870, https://doi.org/10.1002/wcc.147.

Zolina, O., C. Simmer, K. Belyaev, S. K. Gulev, and P. Koltermann, 2013: Changes in the duration of European wet and dry spells during the last 60 years. *J. Climate*, **26**, 2022–2047, https://doi.org/10.1175/JCLI-D-11-00498.1.

Zong, Y., and X. Chen, 2000: The 1998 flood on the Yangtze, China. *Nat. Hazards*, **22**, 165–184, https://doi.org/10.1023/A:1008119805106.

Zscheischler, J., and Coauthors, 2020: A typology of compound weather and climate events. *Nat. Rev. Earth Environ.*, **1**, 333–347, https://doi.org/10.1038/s43017-020-0060-z.